Journal of Orthopaedic Translation 49 (2024) 1–10

Contents lists available at ScienceDirect

Journal of Orthopaedic Translation

journal homepage: www.journals.elsevier.com/journal-of-orthopaedic-translation

Original Article

Failure analysis and design improvement of retrieved plates from revision surgery

Ning-Ze Zhang [a,b,e], Yang-Yang Shui [b], Qi-Da Zhang [a,e], Yuan-Tao Zhang [a,e], Jian Su [b,c], Ling Qin [a,e,**], Cheng-Kung Cheng [d,*]

[a] Musculoskeletal Research Laboratory, Department of Orthopaedics & Traumatology, The Chinese University of Hong Kong, Hong Kong SAR, 999077, China
[b] Key Laboratory of Biomechanics and Mechanobiology, Ministry of Education, Beijing Advanced Innovation Center for Biomedical Engineering, School of Biological Science and Medical Engineering, Beihang University, Beijing, 100083, China
[c] Beijing Institute of Medical Device Testing, Beijing, 101111, China
[d] School of Biomedical Engineering, Shanghai Jiao Tong University, Shanghai, 200030, China
[e] Innovative Orthopaedic Biomaterial and Drug Translational Research Laboratory, Li Ka Shing Institute of Health Sciences, The Chinese University of Hong Kong, Hong Kong SAR, 999077, China

ARTICLE INFO

Keywords:
Biomechanical performance
Bone plate
Design improvement
Failure analysis
Magnesium

ABSTRACT

Background: The fracture of bone plate can cause considerable pain for the patient and increase the burden on the public finances. This study aims to explore the failure mechanism of 49 plates retrieved from revision surgery and introduce pure magnesium (Mg) block to improve the biomechanical performance of the plate via decreasing the stiffness and to stimulate the biological response of the plate potentially by the degradation of Mg block.
Methods: The morphological analysis and component analysis of the plates were conducted to determine the fracture reason of the plates combining the clinical data. According to the structural feature, the 49 retrieved plates were divided into: traditional plate (TP), asymmetrical plate (AP), reconstructive plate (RP) and central enhancement plate (CEP), and their structure features are normalized in a commercial plate, respectively. The biomechanical performance of the plates was evaluated using a validated femoral finite element model. A block of pure Mg with a thickness of 1 mm, 1.5 mm and 2 mm was also incorporated into the CEP to be assessed.
Results: The results indicated that the retrieved plates mainly failed due to fatigue fracture induced by delayed union or nonunion (44/49), and using pure titanium plates in weight-bearing areas increased the risk of fracture compared with Ti alloy plates when the delayed union or nonunion occurred. The TP demonstrated the highest compression resistance and bending resistance, while CEP had the highest rotational resistance. As the thickness of the Mg block was increased, the stress on the plate in compression decreased, but the stress in rotation increased. The plate with a 1.5 mm Mg block demonstrated excellent compression resistance, bending resistance and rotational resistance.
Conclusion: Fatigue fracture resulting from the delayed union or nonunion is the primary failure reason of plates in clinic. The incorporation of Mg block into plate improves the biomechanical performance and has the potential to promote bone healing. The plate with a 1.5 mm Mg block may be suitable for use in orthopaedics.
The translational potential of this article: This study assessed the failure mechanism of retrieved bone plates and used this data to develop a novel plate incorporating a 1.5 mm block of pure Mg block at the position corresponding to the fracture line. The novel plate exhibited excellent compression resistance, bending resistance and rotational resistance due to the alleviation of stress concentrations. The Mg block has the potential to degrade over time to promote fracture healing and prevents fatigue fracture of plates.

* Corresponding author. School of Biomedical Engineering, Shanghai Jiao Tong University, Shanghai, 200030, China.
** Corresponding author. Department of Orthopaedics and Traumatology, The Chinese University of Hong Kong, Hong Kong SAR, 999077, China.
E-mail addresses: lingqin@cuhk.edu.hk (L. Qin), ckcheng2020@sjtu.edu.cn (C.-K. Cheng).

https://doi.org/10.1016/j.jot.2024.08.011
Received 10 August 2024; Accepted 14 August 2024
Available online 27 September 2024

1. Introduction

Violence and long-term cumulative damage from strain are common causes of bone fractures [1]. Fracture of long bones due to trauma has the highest incidence with a rate of 3.21 per thousand persons [2]. Bone plates are often used to connect and reconstruct the broken bones and play a critical role in securing the bone fracture so the patient can place limited weight on the bone to promote fracture healing. However, fracture of bone plates is not uncommon and can lead to considerable pain for the patient and place a burden on public finances.

The survivorship of the plate is highly dependent on the material, structure, and trauma-based application [3]. Stress or strain states related to the bearing capacity are used to predict the failure of the plate. Clinical experiments have shown that the maximum stress on the plate is mainly concentrated near the fracture line of the bone [4], and empty hole (without positing screw) of the plate is the main fracture site due to the presence of holes weakening the strength of the plate [5]. Optimizing the material and design of the plate can improve the strength and alleviate stress concentrations to reduce the risk of fracture.

Stainless steel, titanium (Ti) and Ti alloys are the most common materials for bone plates, while degradable polymers and metals that can stimulate specific cell responses to accelerate fracture healing are gaining ground and can potentially avoid the need for a second surgery to remove the implant [6]. Equally important, the structural features of the plate fixation system can have a considerable impact on the longevity and success of the implant, including the shape of the plate, the distribution of the holes, and the position of the screws. Plate fixation systems has experienced the dynamic compression plate (DCP), limited contact-DCP, less invasive stabilization system, and formed the universal locking compression plate (LCP) [7]. LCP, which combines compression holes and locking holes, gives surgeons the choice to use either compression screws or locking screws during the surgery, according to the specific fracture. Limited by the shape of the plate matched the bone, LCP combined width of the holes equaled the width of the plate is developed, which is known as the reconstructive plate [8]. So far, LCPs are classified as either broad plates (asymmetrical holes) or narrow plates (symmetrical holes), with different distributions of holes aimed to accommodate different fracture types. Firoozabadi et al. reported that filling the unused combination locking/compression holes in the bridging osteosynthesis does not increase the stiffness and fatigue lifetime of the plate fixation system [9]. However, the integrated design without reserving the empty hole of LCP corresponding to the bone fracture area induces more uniform stress distribution and smaller peak stress on the plate [10]. Aside from the design of the plate, the placement of the screws in the plate during the fixation is also nonnegligible for stability [11]. Ei Maraghy et al. [12] found that when screws were inserted into the screw holes at both ends of the plate, the torsional stiffness of the plate was significantly improved. The screw density should be less than 40 %~50 % of the plate when the plate is used for internal fixation [13]. At the same time, to alleviate stress concentrations on the plate near the fracture line, 2–3 empty holes should be left near the fracture line during surgery to reduce the risk of plate fracture [14]. However, an insufficient number of screws can lead to an unstable fixation and require revision. Though numerous plates have been used in clinical settings over several decades, the effect of structure features on failure is still lacking overall understanding and novel material to promote bone fracture healing is also needed.

This study aims to explore the failure mechanism of 49 retrieved bone plates from revision surgery and, using the data collected, propose a new design with Mg block to protect the plate from fracture. The clinical data was collected and morphology analysis was conducted to distinguish the fracture reasons of the retrieved plates. According to the distribution of the holes and the feature of the plates, 49 retrieved plates were divided into 4 types: traditional plate (TP), asymmetrical plate (AP), reconstructive plate (RP), central enhancement plate (CEP), and their structural features were normalized in a commercial plate, respectively. The biomechanical performance of the plates was assessed in a validated femoral finite element model. Finally, the magnesium (Mg) block was introduced to the CEP to improve the biomechanical performance and potentially accelerate bone healing.

2. Materials and methods

2.1. Clinical data collection

This study investigated 49 bone plates retrieved from revision surgery at local hospitals (Beijing and Xi'an), which collected by Beijing Municipal Medical Products Administration. There were 32 male patients and 17 female patients with an age range of 16–92 (average ± SD: 49.16 ± 15.80). The survivorship of the plates was no more than 3 months (average ± SD: 2.2 ± 1.10) in 5 cases, between 3 months and 6 months (average ± SD: 4.43 ± 0.53) in 7 cases, and longer than 6 months (average ± SD: 20.94 ± 14.79) in 37 cases. The implanted sites of plates covered the tibia, fibula, femur, clavicle, humerus, cubitus and radius. The fracture sites were classified by the fracture line (Fig. 1A), working length (the distance between the two screws closest to the fracture site) excluding the fracture line (Fig. 1B), and hole posited screw (Fig. 1C). The 49 plates were categorized into 4 types according to the distribution of screw holes and the shape of the plate. According to the screw hole distribution, the plates can categorize as either symmetrical plates, with holes laid out along the center line of the long axis of the plate, or asymmetric plates (AP) with holes laid out on both sides of the center line of the plate. Symmetrical plates with locking or compression holes were identified as 'TP' in this study, plates without holes near the fracture site were identified as 'CEP', and if the combined width of the holes equaled the width of the plate this was identified by 'RP' (Table 1). Examples of the retrieved bone plates are shown in Fig. 1D–G, and some typical clinical cases associated with these failures are as follows.

Case 1 (TP): The patient suffered an open comminuted fracture of the left tibia and fibula caused by an accident, and underwent open reduction and internal fixation (ORIF) with allograft bone grafting. Weight-bearing began 3 months after the operation, and the plate fracture was identified by radiography at 5 months and diagnosed as non-union. The fractured plate was retrieved during revision surgery (Fig. 1D).

Case 2 (AP): The patient fractured the right femur due to a fall and received ORIF. Postoperative radiographs showed good alignment of the fracture, stable internal fixation, and postoperative incision healing. One month after the injury, the patient complained of swelling, deformity and pain in the right femur. X-ray examination indicated a fracture of the plate. The fractured plate was retrieved during revision surgery (Fig. 1E).

Case 3 (RP): The patient injured the right forearm and complained of pain, swelling and limited movement. The diagnosis was a right ulnar fracture which was treated with ORIF. At approximately 4 months after operation, bone nonunion was identified and the internal fixation was found to have failed. The fractured plate was retrieved during revision surgery (Fig. 1F).

Case 4 (CEP): The patient suffered a fracture of the left tibia caused by an accidental collision while running and received surgical treatment. Seven months later, the patient felt the fracture site moved slightly. X-ray examination showed postoperative changes in the left tibial fracture and the internal fixation was found to have failed (Fig. 1G).

2.2. Fracture morphological analysis of the retrieved plates

An analysis of the fracture morphology was performed to identify the failure mode of the plates. The fractured part region of the plates was cut and cleaned with distilled water. Subsequently, the samples were evaluated by a field emission scanning electron microscope (FESEM, Zeiss ULTRA PLUS, Germany) in a vacuum environment of argon with an

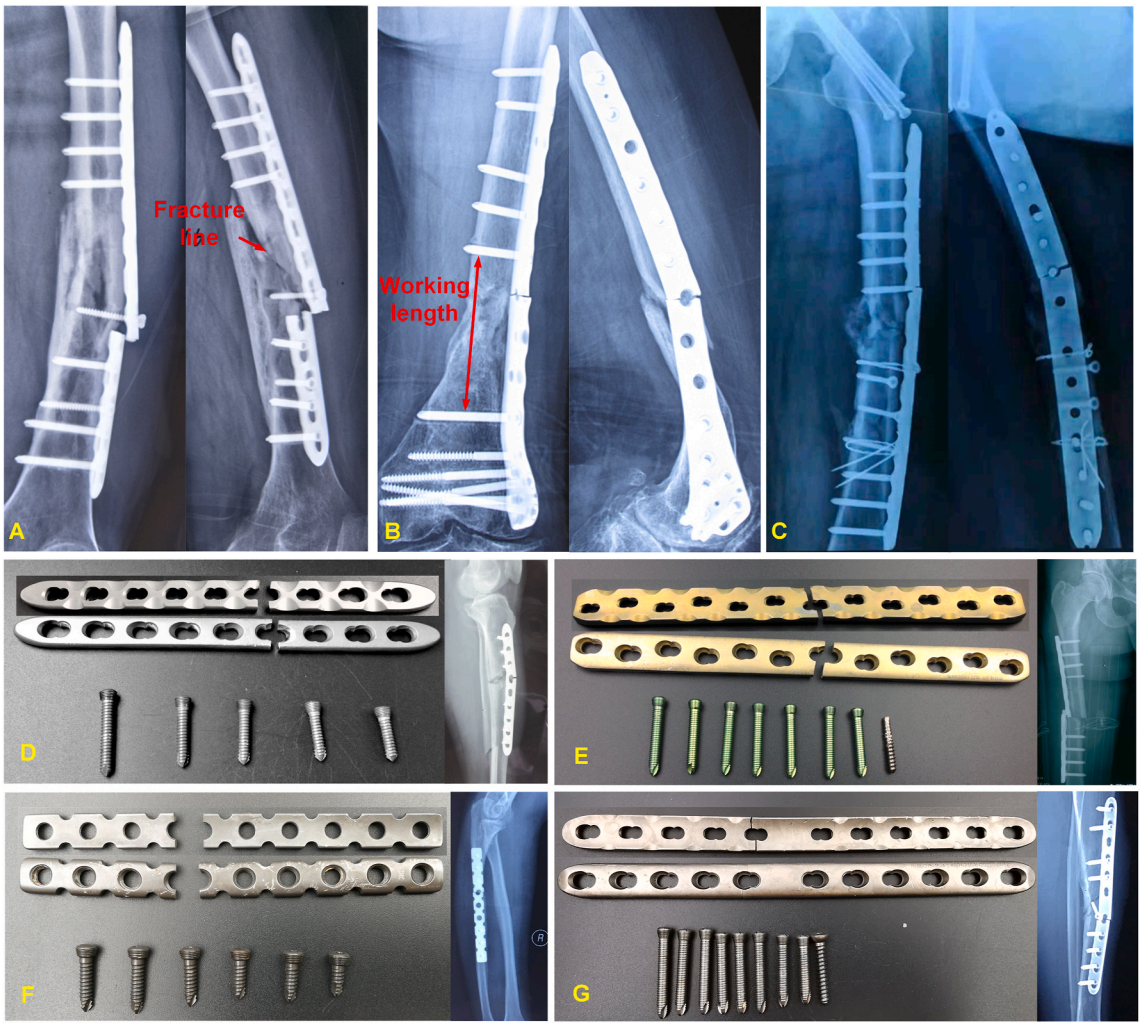

Fig. 1. X-ray of patients and retrieved bone plates. (A) Plate failed at the fracture line (B) Plate failed within the working length (C) Plate failed at the hole posited the screw (D) Traditional plate (E) Asymmetric plate (F) Stress dispersed plate (G) Central enhancement plate.

Table 1
Information on patients and the retrieved plates.

Classification		Magnitude
Gender	Male	32
	Female	17
Age/Year	49.16 ± 15.80	
Survivorship/Month	≤3 (average ± SD: 2.2 ± 1.10)	5
	3-6 (average ± SD: 4.43 ± 0.53)	7
	>6 (average ± SD: 20.94 ± 14.79)	37
Implanted site	Tibia	12
	Femur	19
	Clavicle	5
	Humerus	6
	Cubitus	4
	Radius	2
	Fibula	1
Fractured site	Fracture line	26
	Working length exclude fracture line	9
	Hole posited screw	14
Type of plate	Traditional plate, TP	21
	Asymmetric plate, AP	10
	Reconstructive plate, RP	11
	Central enhancement plate, CEP	7

acceleration voltage of 10 kV. Energy disperse spectroscopy (EDS) was then used to distinguish the chemical components of the plates.

2.3. Normalization of the fractured plates and biomechanical analysis

After extracting the structural features of the fractured plates, this study selected a common TP as the basic plate (control group) (Naton, Beijing, China) to normalize the parameters of the fractured plates. The basic plate had dimensions of 240 × 18 × 4.5 (L × W × H) mm and 13 holes with a diameter of 5.5 mm, and the distance between the holes was 18 mm (Fig. 2Aa). The locking screws were 7 mm long and had a diameter of 5 mm. For simplification, the screw threads were removed. Measurements for the plate and screws were gathered by reverse engineering and were then reconstructed in SolidWorks 2014 (Dassault Systemes S.A, France). Another three structures of the fractured plates used in this study were also developed. Except for the different topological features, all other parameters, such as length, width and thickness, were the same (Fig. 2Ab-d) to control the variables. The inserted positions of the plates and screws on the femur was guided by a senior surgeon and the implantation process was achieved by a Boolean operation between the implants and bone (Fig. 2B).

The femoral finite element model was constructed from a healthy volunteer with approval from the Institutional Review Board (K2021066), which had been validated in our previous research according to the strain and displacement gauged by the strain gauge [15,

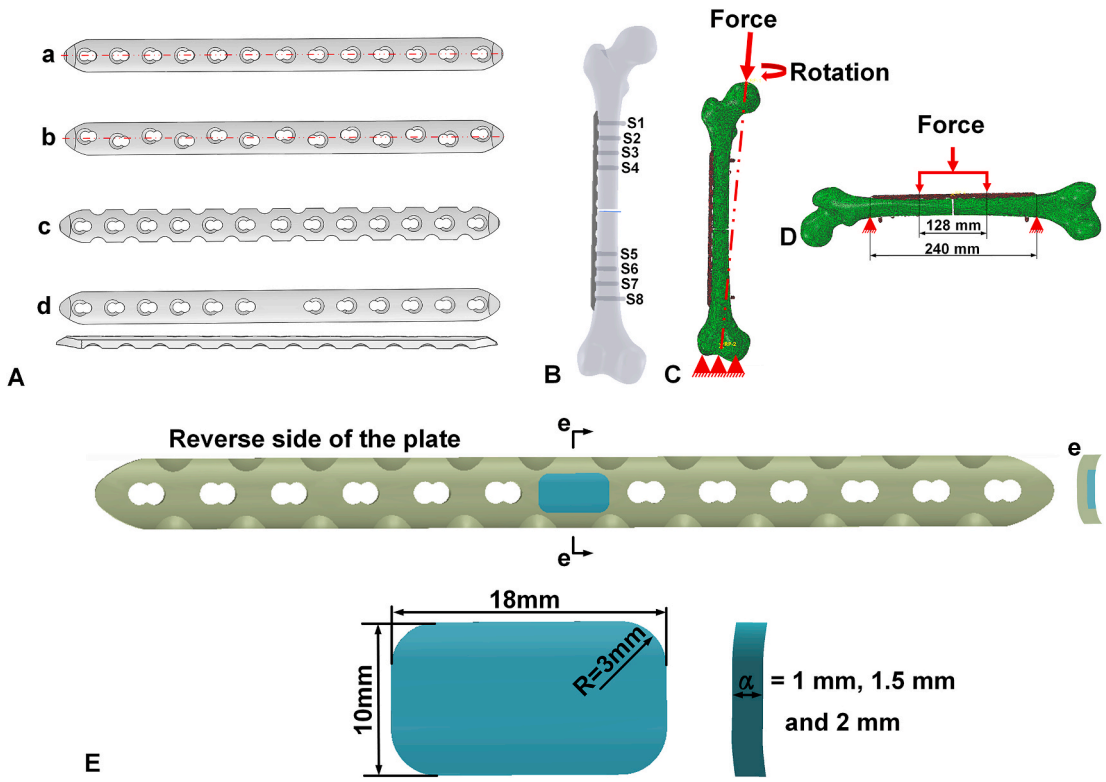

Fig. 2. (A) The structure of the simulated plates: a. traditional plate (TP) b. asymmetric plate (AP) c. reconstructive plate (RP) d. central enhancement plate (CEP), (B) Assembly model of the bone and fixation system (C) Compression model and rotation model (D) Four-point bending model from lateral side to medial side (E) Improvement of plate with a block of pure Mg, e. cross section of the plate. A cross-sectional view (e–e) of the improved plate shows the interface of plate and Mg block.

16]. Mesh size and convergence analysis were performed, where the element size was gradually reduced (4 mm, 3 mm, 2 mm and 1 mm) until the maximum Von Mises stress converged at 2 mm. A biomechanical simulation was conducted in Abaqus 2016 (Dassault Systèmes Simulia Inc, France). The material properties of the bone were assigned in Mimics 17.0 (Materialise, Leuven, Belgium) according to the gray values of the bone from CT images. The material properties of the bone were assigned in Hounsfield units (HU) using the following equations [17–19]:

$$\rho_{eqm} = 10^{-3}\,(\mathrm{a} \times \mathrm{HU} - \mathrm{b})\ \left(\mathrm{g}/\mathrm{cm}^3\right) \quad (1)$$

$$\rho_{ash} = 1.22\,\rho_{eqm} + 0.0523\ \left(\mathrm{g}/\mathrm{cm}^3\right) \quad (2)$$

$$E_{\mathrm{cort}} = 10200 \times \rho_{ash}^{2.01}\ (\mathrm{MPa}) \quad (3)$$

$$E_{\mathrm{trab}} = 5307\,\rho_{ash} + 469\ (\mathrm{MPa}) \quad (4)$$

ρ_{eqm} and ρ_{ash} are the equivalent mineral density of bone and the ash density of the bone, and E_{cort} and E_{trab} are the Young's moduli of the cortical and trabecular regions, respectively. The parameters a and b in equation (1) were determined by phantoms in the CT images. The plate and screws were made of Ti alloy (Ti_6Al_4V) with a Young's modulus of 110 GPa and Poisson's ratio of 0.3. A 3 mm bone gap was created at the center of the femur to simulate a fracture [20]. Four fixation systems (plate and screws) were inserted in the femur to assess their biomechanical performance. A reference point was set at the center of the femoral head and coupled with the surface of the femoral head as the point of force application. The distal femur was constrained in all degrees of freedom during the compression and rotation tests. The patient's body weight was assumed to be 60 kg and compression loads of 600 N and 1500 N (2.5 times body weight) were applied to the femoral head from the proximal end of the femur to the distal end of the femur along the axis of the femur, respectively [21] (Fig. 2C). A torque of 10 Nm was also applied to the femoral head to test the rotation properties of the plate fixation system [22] (Fig. 2C). To assess the bending behavior, a force of 1000 N was applied along the direction from the lateral femur to the medial femur [23]. The proximal femur and distal femur were fixed with the span of length of plate (240 mm), and the force was conducted at the middle of the plates with a span of 128 mm (half of the plate length add a distance between two holes) during the bending simulation (Fig. 2D). The following friction coefficients were applied to contact surfaces: 0.3 between the bone and LCP [24], 0.46 for bone–bone interactions [25], and 0.23 between the screws and LCP [26]. Bone-screw interfaces were assumed to be tied. The biomechanical performance of the plate and screws were recorded when the plate fixation system was placed under compression, rotation and bending.

2.4. Improvement in plate design and biomechanical analysis

Combining with the clinical data and the structural features of the plates, a block of pure Mg was inserted into the center of the CEP corresponding to the fracture area under the ideal condition to reduce its modulus. The degradation of the Mg aimed to adjust the synthesis and release of the calcitonin gene-related peptide around of the trauma area to accelerate fracture healing [27]. The length of the block corresponded to the width of the plate (18 mm), and the block had a width of 10 mm. The thickness of the block would have a direct effect on the stability of the plate fixation system. To determine the optimal thickness, three different values (1 mm, 1.5 mm and 2 mm) were assessed. The upper and lower surfaces of the block coincided with the back profile of the plate (Fig. 2E). In fact, the Mg block was inserted into the interspace of the plate and these devices were separated to manufacture and experienced the cutting and milling. To achieve the stable bonding between the plate and Mg block, the interference fit was set, which means that the size of

Mg block is larger than the interspace of the plate by around 0.2 mm. In the finite element model, the Mg block was bonded to the plate to simulate the interference fit between the Mg block and plate and avoid the fall off of the Mg block during the operation. The biomechanical analysis was conducted using the method previously described.

3. Results

3.1. Assessment of retrieved plate

As shown in Table 2, 44 of the retrieved plates had fractured due to delayed union or nonunion. In particular, one case with bowing of the femur affected the stability of the plate fixation system and caused nonunion. With respect to the materials, 38 plates were made of pure Ti, 6 plates were made of Ti_6Al_4V, and the rest plates were made of stainless steel. The tensile strength of pure Ti is 240–550 MPa [28], much lower than that of Ti_6Al_4V, which increases the fracture risk when used in the weight-bearing bones, such as the femur and tibia. The fracture modes of the retrieved plates were fatigue fracture and quasi-cleavage fracture.

3.2. Fracture morphology of the retrieved plates

Fatigue fracture occurred in 46 cases, and the remaining 3 cases failed by a quasi-cleavage fracture (Table 2). Fig. 3 shows the typical fracture morphology of plates made of stainless steel (316L), Ti_6Al_4V and Ti. The morphology of stainless steel indicated the features of quasi-cleavage fracture, which contained a river line, cleavage facets, tear edges and a ligulate pattern. Though Ti_6Al_4V also showed a river line, the fatigue striations had a distinct direction. During crack propagation, the micropore coalescence formed a dimple and it was classified as a fatigue fracture. The morphology of pure Ti plates all exhibited distinguishing features of fatigue fracture, including fatigue striations and secondary cracks.

3.3. Biomechanical performance of the normalized retrieved plate fixation systems

Fig. 4 shows the stress distribution on the plate fixation systems. Under a load of 600 N, the maximum stress on AP and TP appeared at the position corresponding to the fracture line, while the maximum stress on RP occurred at the 6th hole. Similarly, for CEP, the fracture line area was reinforced by the solid region of the plate and the position of the empty hole (6th hole) carried the maximum stress. The red arrow in Fig. 4A indicates the specific location of maximum stress, and the maximum stress on AP, RP and CEP increased by 0.53 %, 14.00 % and 3.95 %, respectively, in comparison to TP. Increasing the load to 1500 N resulted in the maximum stress on all plates shifting to the femoral proximal 5th hole (Fig. 4B). The maximum stress on AP, RP and CEP increased by 8.00 %, 21.78 % and 4.42 %, respectively, in comparison to TP. Whether loaded with 600 N or 1500 N, the RP model displayed the highest stress of all plates and TP had the lowest stress (Fig. 4C). The CEP had a better carrying capacity at higher loads than AP and RP. From the stress distribution of the screws, the S4 and S5 screws at both ends of the working length were subjected to greater stress, and the stress on the proximal screw (S4) was higher than the distal screw (S5). The stress on S4 was approaching that of S5 for AP, indicating a more stable fixation around the fracture line. Meanwhile, S2 and S7 had lower stress under the load of 600 N. The construct stiffness of CEP was highest among the retrieved plates, with a stiffness of up to 84.85 N/mm (Table 3). The RP yielded the lowest construct stiffness, with a value of 70.85 N/mm. To summary, the TP demonstrated the great compressive properties.

Fig. 5 shows the stress of the plates when placed in rotation and bending. The CEP bore the lowest stress in rotation, followed by TP, AP, and RP, indicating that the CEP had excellent torsional resistance. Under bending, when the load was applied from the lateral side to the medial side, the TP model carried the lowest force and AP carried the highest force. In general, the TP displayed the best performance in bending, while RP and CEP had similar bending resistance.

Table 2
Failure reasons of retrieved plates from revision surgery.

Failure information		Magnitude
Healing status	Delayed union	7
	Non-union	37
	Others	5
Materials	Pure Ti	38
	Ti_6Al_4V	6
	Stainless steel	5
Fracture mode	Fatigue fracture	46
	Quasi-cleavage fracture	3

3.4. Biomechanical performance of the improved plate fixation system

Fig. 6 shows the biomechanical performance of the plate incorporating the pure magnesium block (Mg-CEP). Replacing a section of the Ti alloy plate with pure magnesium reduced the maximum stress on the plate when placed in compression (Fig. 6A). As the thickness of the Mg block increased, the maximum stress on the plate tended to decrease. When the thickness of the Mg block was 1.5 mm, the stress on the plate was 1.13 % and 0.52 % greater than the TP when placed under 600 N and 1500 N loads, respectively. Increasing the thickness of the Mg block to 2 mm resulted in a stress that was 99.9 % and 98.6 % of the TP. However, the stress on the plate in rotation increased with the thickness of the Mg block. Compared with the 1 mm Mg block, the 1.5 mm Mg block resulted in an increase in stress of 0.72 %, while the 2 mm Mg block increased the stress by 22.04 %. When loaded with a lateral to medial force, the stress on the Mg-CEP was lower than all of the other plate including retrieved plates and improved plates. It is worth noting that the plate with a thickness of 1.5 mm had the lowest stress in bending, reaching 44.77 MPa (Fig. 6B). Under the load of 1500 N, the compressive stress was transferred from the proximal femur to the plate fixation system and return to the distal femur (Fig. 6C). In the region of positing the screws, the bone and screws carried the load together, while the plate bore the primary force in the working length. Fig. 6D shows the stress distribution on the Mg block with various thicknesses under compression (1500 N) and rotation. The stress on the Mg block increased with its thickness. In compression, when the thickness was set to 1 mm, the stress was mainly distributed at the longitudinal edge, indicating that the Ti alloy regions of the plates were the main bearings. Increasing the thickness of the Mg block to 1.5 mm and 2 mm caused the maximum stress to shift to the transverse edge, indicating that the Mg block was squeezed by the Ti alloy plate. In particular, the block was subjected to greater stress in rotation, illustrating the intense interaction between the plate and the block. The plate bore almost all stress in rotation at the location of working length (Fig. 6E).

Table 3 shows the construct stiffness of the improved Mg-CEP fixation system. The introduction of the Mg block reduced the construct stiffness of the plate fixation system in comparison to the CEP. As the thickness of the Mg plate increased, the construct stiffness tended to decrease, reaching 80.19 N/mm, 78.45 N/mm and 77.75 N/mm for the 1 mm, 1.5 mm and 2 mm plates, respectively. The construct stiffness of the plate with a 1.5 mm Mg block was similar to the plate with a 2 mm Mg block, but was 7.54 % lower than the strongest retrieved plate (CEP).

4. Discussion

This study aimed to investigate the failure mechanism of bone plates retrieved during revision surgery and, with this knowledge, introduced the pure Mg block to improve the biomechanical performance and stimulate the bone healing potentially. The results indicated that the retrieved plates mainly suffered fatigue fracture induced by delayed union or nonunion (44/49) and pure Ti plates used in weight-bearing

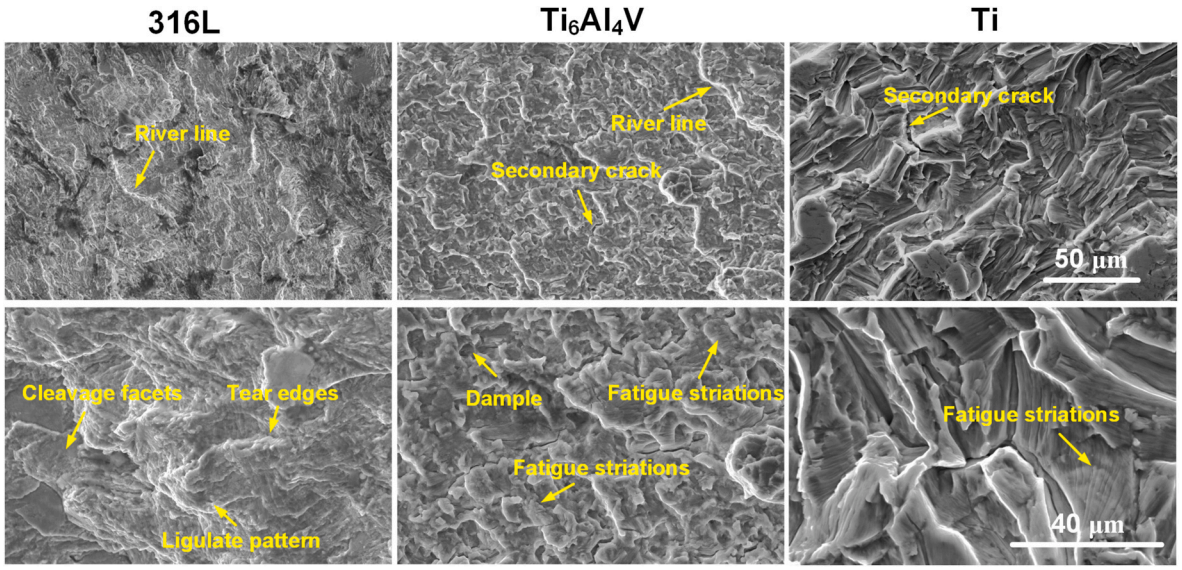

Fig. 3. Typical fracture morphology of plates.

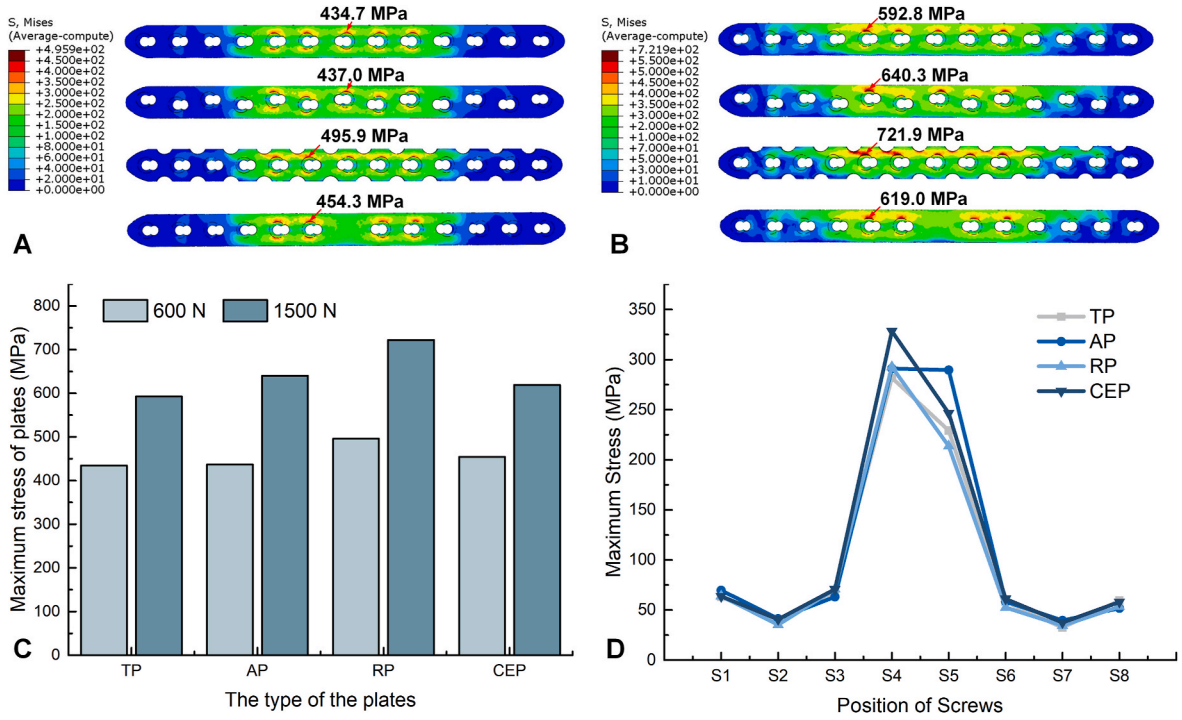

Fig. 4. The stress distribution on the plate fixation systems in compression. (A) Stress distribution when loaded with 600 N (B) Stress distribution when loaded with 1500 N (C) Maximum stress on the plates in compression (D) Maximum stress on the screws when loaded with 600 N.

Table 3
The construct stiffness of the plate fixation systems.

Plate types	Stiffness (N/mm)
TP	71.35
AP	73.51
RP	70.85
CEP	84.85
Mg-CEP-1 mm	80.19
Mg-CEP-1.5 mm	78.45
Mg-CEP-2 mm	77.75

areas increased the risk of fracture compared with Ti alloy plates when the delayed union or nonunion occurred. The TP was found to have favorable compression resistance and bending resistance, while the CEP was better able to resist rotation. As the thickness of the block increase, the stress on the plate in compression decreased, while the stress in rotation increased. The plate with a 1.5 mm Mg block demonstrated excellent compression resistance, bending resistance and rotational resistance, indicating the potential application in orthopaedics to bear the weight and promote bone healing conceptually.

Analyzing retrieved plates is important for understanding the failure mechanism and improving the design. In emergency trauma situations, the choice of implant is limited by what the hospital has in stock, while the treatment options and surgical approach are determined by the

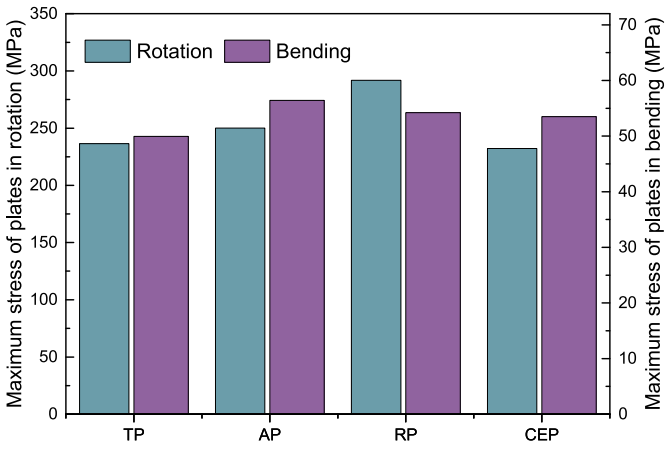

Fig. 5. The maximum stress on the plate fixation systems under rotation and bending.

surgeon [29]. Regardless of the plate used, the aim should be to bear the majority of the load until bone union is achieved. Bone union may be influenced by many aspects, including the physiological condition of the patient, the biomechanical environment, and post-operative complications such as infection [30]. Delayed union is described as a lack of radiographic evidence of healing at 3–6 months after injury, while non-union may be diagnosed after 6 months and then verified after another three months, according to the FDA definition. The occurrence of non-union depends on the fracture location: tibial fractures have the highest incidence (0–15 %), followed by humeral fractures (0–13 %) and femoral fractures (1–11 %) [31]. In this study, 75.51 % (37/49) of cases displayed nonunion and 14.29 % (7/49) displayed delayed union. These percentages are higher than the clinical statistic results because the plates had cracked and delayed union or nonunion was a crucial reason for plate fracture. Previous studies have similarly reported that 75 % of implant failures occur within 3 months of operation and 50 % occur after 6 months due to plate fatigue, secondary to delayed union, and continuous movement of the fracture site [32].

To simulate the delayed union and nonunion, the transverse fracture was developed in this study and the fracture gap was 3 mm. The geometric shape of fracture surfaces significantly affects the stress distribution on the plates [33]. The individualized natural fracture models could provide more accurate results for internal fixation strategy in clinics [34]. However, the plates in this study were expected to bear the physical load under uncertain fracture. Previous research investigated the effect of facture topology on the stress distribution on plate and indicated that the acute angle of 76° (long oblique fracture) resulted in lower von Mises stress on the plate compared with the obtuse angle of 146° (short oblique fracture) [35]. The stress of the transverse fracture (90°) used in this study was within the range of long and short oblique fractures. In addition, the gap size also plays a significant role in the stability of fracture fixation systems and higher gap sizes lead to less stable fixation constructs [36]. The 3 mm bone gap used in this study is commonly adopted in previous literature [37]. In the plate-fixation system, as the body weight is transmitted through the plate, this causes greater stress on the plates and eventual implant failure. Pure Ti is commonly used in implants due to its excellent mechanical properties and biocompatibility. However, the tensile strength of pure Ti is lower than Ti alloys and the fatigue mechanism of pure Ti has been associated with intense secondary intergranular cracking (brittle fracture) (Fig. 4). Implants made of pure Ti are susceptible to breakage if bone consolidation is delayed [38].

The 49 retrieved plates assessed in this study could be categorized into 4 design types (TP, AP, CEP, RP) and extracted the features and normalized them against a commercial plate. The mechanical performance of the 4 plates designs was assessed using finite element analysis. When loaded with a 600 N compression force, the maximum stress was located close to the fracture line with the TP and AP, which is also consistent with the fracture sites in cases 1 and 2 detailed in section 2.1.

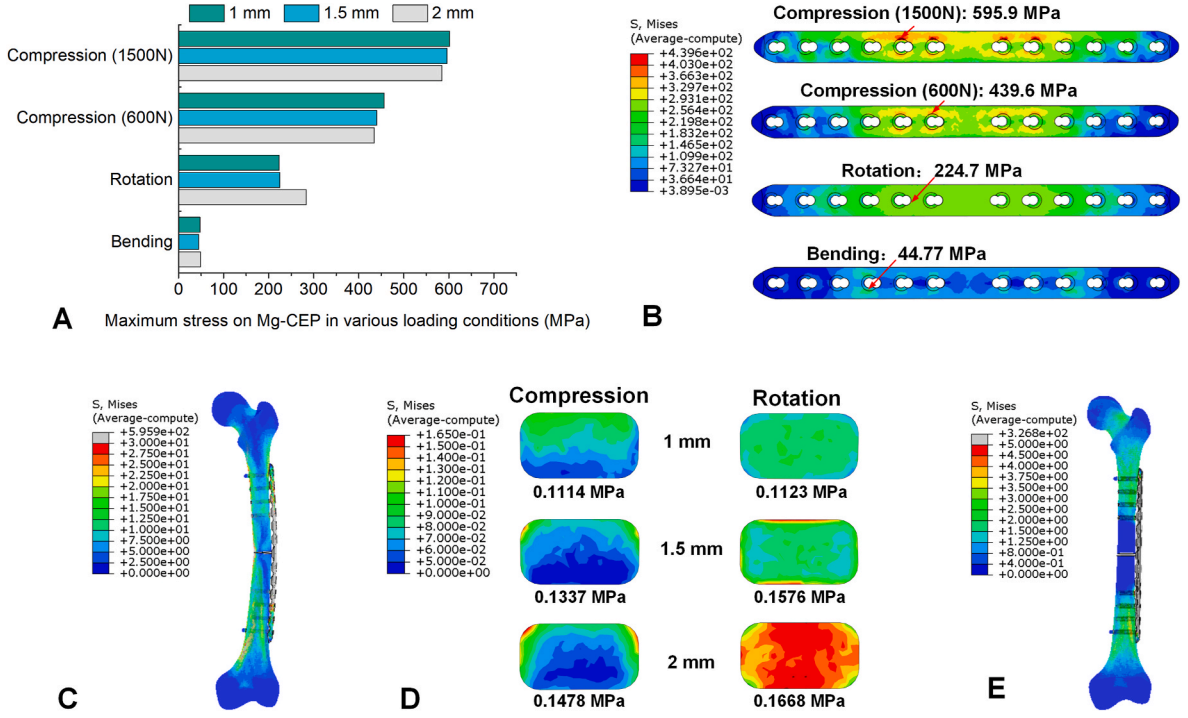

Fig. 6. The biomechanical performance of the improved plate fixation system (Mg-CEP). (A) Maximum stress on the Mg-CEP in various loading conditions (B) Stress distribution on the Mg-CEP with a 1.5 mm block (C) Stress distribution on plate fixation system with a 1.5 mm Mg block in compression of 1500 N (D) Stress distribution on the Mg block with various thicknesses under the condition of compression and rotation (E) Stress distribution on plate fixation system with a 1.5 mm Mg block in rotation.

Stoffel et al. [39] also investigated the performance of a locking compression bone plate and found that the peak stress on the bone plate was located at the inner screw hole near the fracture line. Due to the nonunion, the plates bore the impact load over a prolonged period which eventually caused failure by fatigue fracture. However, the RP model showed the maximum stress at the screw hole in the working length excluding the fracture line. This was likely due to the lower stiffness of the RP construct (Table 3). Under the same loading condition, the RP was more flexible with a gap between the fractured bone surfaces, and transmitted the stress to the adjacent hole to induce the maximum stress. A retrospective cohort study found that the incidence of reoperation with RP was higher than other plate designs due to its lower strength [40]. Due to the absence of screw holes near the fracture line, the maximum stress on the CEP model transferred to the hole closest to the fracture line, which corresponded to the description of case 4. Under a load of 1500 N, the maximum stress all presented in working length exclude fracture line, similar to the Fig. 1B. This may be explained that the bilateral fracture bones were contacted under the load of 1500 N and the greater load deforming the plates to transfer the maximum stress to adjacent vulnerable sites. The TP model demonstrated better compression resistance and bending resistance than the other plates depending on structural characteristics in this study. Muthusamy et al. [41] revealed that plates with offset holes, similar to AP, increased the plate stress by 8.08 % compared with plates with combi holes (TP). Moreover, the fatigue life of plates is significantly decreased with offset holes.

The retrieved plates showed that the plates failed predominantly at the screw hole near the fracture line and the fracture mode was fatigue fracture. Removing the screw holes around the center of the plate to make a solid region was of great significance to improve the fatigue strength of the plate. Of the retrieved plates, 7/49 were CEPs which failed because the local enhancement of the plate in CEP caused the weaker site in the CEP fixation system. Homogenizing the stress in CEP under the different loading conditions and promoting bone healing were the optional strategy. This study incorporated a block of pure Mg into the CEP to reduce the structural modulus at the area of the fracture line and reduce the construct stiffness of the plate fixation system to alleviate stress concentrations (Table 3). As the thickness of the block was increased, the stress on the plate in compression decreased, while the stress in rotation increased. Increasing the thickness of the block also reduced the stiffness of the working length which resulted in stress transferring from the proximal portion to the distal portion, thus lowering the maximum stress on the plate. In rotation, the reinforced region of the plate acted as the bearing zone, and reducing the stiffness of the plate increased the maximum stress. Using a 2 mm Mg block noticeably reduced the rotational resistance (Fig. 6A) which would likely increase the risk of fracture. The Mg-CEP with a 1.5 mm Mg block (33.33 % of the plate thickness) balanced the stress distribution in compression and rotation, while the maximum stress increased by 1.13 % and 0.52 % under the loads of 600 N and 1500 N, respectively, and decreased by 4.95 % and 10.41 % in rotation and bending comparing with the TP. Except for the plate design in this study, the porous structure is also the potential choice to reduce the stress shielding. Takizawa et al. [42] proposed a porous Ti fiber plate with similar elastic modulus to bone cortex. The bone tissue would grow into the porous structure to achieve the integration between the plate and adjacent bone without a secondary operation for implant removal. Therefore, the porous structure of plate incorporating magnesium ions may achieve the same outcome.

The Mg block not only improved the stress distribution on the CEP model, but would also be beneficial for promoting bone healing as the block degrades over time [43]. Mg is the fourth most prevalent mineral in the human body, with about 60 % of the content stored in bones and about 30 % in muscles to maintain functionality of the musculoskeletal system [44]. Previous studies have shown that the release of Mg ions promotes the substantial generation of local neuronal calcitonin gene-related polypeptide to accelerate bone-fracture healing [45]. Meanwhile, Mg ions also induce neurite outgrowth in a concentration-dependent manner via the PI3K/Akt signaling pathway and Sema5b to promote nerve regeneration [46]. Chow et al. [47] used an Mg implant to fix a transverse fracture and found that the degradation of the Mg implant improved new bone formation and strengthened the mechanical properties of the repaired bone. In this study, the transverse fracture was conducted to test the stability of the plate fixation system and the degradation of Mg block would also achieve the same healing outcome. Despite of the satisfactory healing effect of Mg implants, the strength of Mg is not enough to support a stable fixation at the bearing site due to the rapid degradation after insertion. This study incorporated the Mg block into the solid part of the plate with a thickness of 1.5 mm to exert the unique superiority of stimulating new bone formation, while the plate fixation system could support the body weight to achieve stable fixation. Similarly, researchers have also proposed using hybrid magnesium-titanium cannulated screws to achieve a stable fixation in vertical femoral neck fractures [48]. Tian et al. adopted Mg screws and Ti fixators to fix a fractured rabbit tibia and found a larger bone callus in the group containing the Mg screws, and the regenerated bone was stronger [49]. Therefore, the CEP with an Mg block proposed in this current study has the potential to accelerate bone fracture healing and reduce stress concentrations on the plate, which would shorten the service time of the plate and reduce the risk of fatigue fracture. In addition, the plate and block are processable and contact stably with the design of interference fit, which supports the orthopaedic translation of this fixation system.

There are some limitations to this study. Only 49 plates were collected in this study and a wider sample size with greater variation would be beneficial to strengthen the findings. In this study, only one fracture type and one screw placement status were studied, and the results may not be completely applicable to the various fracture types observed in clinical practice. The influence of the fracture type and screw positioning on the stress distribution of the plate needs to be further studied. In addition, the degradation of Mg block has the potential to promote bone healing, while the in-vivo test needs to be conducted in the future.

5. Conclusion

This study analyzed the failure mechanism of 49 bone plates retrieved from revision surgery and proposed a novel design with Mg block to promote better bone union. The retrieved plates primarily suffered fatigue fracture induced by delayed union or nonunion, and the pure Ti plates used in weight-bearing areas increased the risk of fracture compared with Ti alloy plates when the delayed union or nonunion occurred. The AP demonstrated favorable compression resistance and bending resistance, while the CEP had better rotation resistance. Incorporating a block of pure Mg improved the compression resistance and bending resistance of the CEP. The CEP with a 1.5 mm Mg block demonstrated excellent compression resistance, bending resistance and rotational resistance and the potential ability to promote bone healing, indicating its promising application in orthopaedics.

Author contributions

Conceptualization, Ning-Ze Zhang, Ling Qin and Cheng-Kung Cheng; Data curation, Ning-Ze Zhang, Yang–Yang Shui and Jian Su; Formal analysis, Ning-Ze Zhang, Yang–Yang Shui, Jian Su and Qi-Da Zhang; Funding acquisition, Ling Qin and Cheng-Kung Cheng; Methodology, Ning-Ze Zhang, Yang–Yang Shui and Cheng-Kung Cheng; Writing - original draft, Ning-Ze Zhang; Writing - review & editing, Ning-Ze Zhang, Yuan-Tao Zhang, Qi-Da Zhang, Ling Qin and Cheng-Kung Cheng. All authors read and approved the final manuscript.

Funding

This work was supported by the National Key Research and Development Projects (Grant number: 2016YFC1101904), Fundamental Research Funds for the Central Universities (AF0820060) and Areas of Excellence from the Research Grants Council of Hong Kong (AoE/M-402/20).

Ethical statements

The retrieved bone plates and relative information used in this study are collected by the Beijing Municipal Medical Products Administration from the hospitals. This belongs to the regular quality supervision of medical institutions to fulfill statutory duties and does not apply to ethical review requirements.

Declaration of competing interest

A conflict of interest occurs when an individual's objectivity is potentially compromised by a desire for financial gain, prominence, professional advancement or a successful outcome. The Editors of the *Journal of Orthopaedic Translation* strive to ensure that what is published in the Journal is as balanced, objective and evidence-based as possible. Since it can be difficult to distinguish between an actual conflict of interest and a perceived conflict of interest, the Journal requires authors to disclose all and any potential conflicts of interest.

Acknowledgments

The authors acknowledge all the participants and participating institutes for experimental and technical support in this study, and Mr. Colin McClean for his assistance with proofreading this manuscript.

References

[1] Hamstra-Wright KL, Huxel Bliven KC, Napier C. Training load capacity, cumulative risk, and bone stress injuries: a narrative review of a holistic approach. Front Sports Act Living 2021;3:665683.
[2] Chen W, Lv H, Liu S, Liu B, Zhu Y, Chen X, et al. National incidence of traumatic fractures in China: a retrospective survey of 512 187 individuals. Lancet Global Health 2017;5:807–17.
[3] Cheng CK, Wang XH, Luan YC, Zhang NZ, Liu BL, Ma XY, et al. Challenges of preclinical testing in orthopedic implant development. Med Eng Phys 2019;72:49–54.
[4] Rao J, Zhang J, Ye Z, Zhang L, Xu J. What is the stable internal fixation for the unstable and osteoporotic supracondylar femoral fractures: a finite element analysis. J Orthop Surg Res 2023;18:759.
[5] Lv H, Chang W, Yuwen P, Yang N, Yan X, Zhang Y. Are there too many screw holes in plates for fracture fixation? BMC Surg 2017;17:46.
[6] Li J, Qin L, Yang K, Ma Z, Wang Y, Cheng L, et al. Materials evolution of bone plates for internal fixation of bone fractures: a review. J Mater Sci Technol 2020;36:190–208.
[7] Tian L, Tang N, Ngai T, Wu C, Ruan Y, Huang L, et al. Hybrid fracture fixation systems developed for orthopaedic applications: a general review. J Orthop Translat 2019;16:1–13.
[8] Xie P, Ouyang H, Deng Y, Yang Y, Xu J, Huang W. Comparison of conventional reconstruction plate versus direct metal laser sintering plate: an in vitro mechanical characteristics study. J Orthop Surg Res 2017;12:128.
[9] Firoozabadi R, McDonald E, Nguyen T-Q, Buckley JM, Kandemir U. Does plugging unused combination screw holes improve the fatigue life of fixation with locking plates in comminuted supracondylar fractures of the femur? J. Bone Joint Surg. Br 2012;94B:241–8.
[10] Yan L, Lim JL, Lee JW, Tia CSH, O'Neill GK, Chong DYR. Finite element analysis of bone and implant stresses for customized 3D-printed orthopaedic implants in fracture fixation. Med Biol Eng Comput 2020;58:921–31.
[11] Mischler D, Windolf M, Gueorguiev B, Nijs S, Varga P. Computational optimisation of screw orientations for improved locking plate fixation of proximal humerus fractures. Journal of Orthopaedic Translation 2020;25:96–104.
[12] ElMaraghy AW, ElMaraghy MW, Nousiainen M, Richards RR, Schemitsch EH. Influence of the number of cortices on the stiffness of plate fixation of diaphyseal fractures. J Orthop Trauma 2001;15:186–91.
[13] Miller DL, Goswami T. A review of locking compression plate biomechanics and their advantages as internal fixators in fracture healing. Clin Biomech 2007;22:1049–62.
[14] Chao P, Conrad BP, Lewis DD, Horodyski M, Pozzi A. Effect of plate working length on plate stiffness and cyclic fatigue life in a cadaveric femoral fracture gap model stabilized with a 12-hole 2.4 mm locking compression plate. BMC Vet Res 2013;9:125.
[15] Zhang NZ, Liu BL, Luan YC, Zhang M, Cheng CK. Failure analysis of a locking compression plate with asymmetric holes and polyaxial screws. J Mech Behav Biomed Mater 2022;138:105645.
[16] Li J, Zhang M, Yao J, Shao L, Fang C, Cheng CK. Risk factors for periprosthetic femoral fractures after cementless total hip arthroplasty. J Arthroplasty 2024;43:1-8.
[17] Les CM, Keyak JH, Stover SM, Taylor KT, Kaneps AJ. Estimation of material properties in the equine metacarpus with use of quantitative computed tomography. J Orthop Res 1994;12:822–33.
[18] Keller TS. Predicting the compressive mechanical behavior of bone. J Biomech 1994;27:1159–68.
[19] Bessho M, Ohnishi I, Matsuyama J, Matsumoto T, Imai K, Nakamura K. Prediction of strength and strain of the proximal femur by a CT-based finite element method. J Biomech 2007;40:1745–53.
[20] Gabarre S, Albareda J, Gracia L, Puertolas S, Ibarz E, Herrera A. Influence of gap size, screw configuration, and nail materials in the stability of anterograde reamed intramedullary nail in femoral transverse fractures. Injury 2017;48(Suppl 6):S40–6.
[21] Chen X, Myers CA, Clary CW, DeWall RJ, Fritz B, Blauth M, et al. Development of axial compression and combined axial compression and torque loading configurations to reproduce strain in the implanted femur during activities of daily living. J Biomech 2021;120:110363.
[22] He Z, Huang S, Ji T, Tang X, Yang R, Guo W. Plate configuration for biological reconstructions of femoral intercalary defect - a finite element evaluation. Comput Methods Progr Biomed 2022;224:107006.
[23] Wisanuyotin T, Sirichativapee W, Paholpak P, Kosuwon W, Kasai Y. Optimal configuration of a dual locking plate for femoral allograft or recycled autograft bone fixation: a finite element and biomechanical analysis. Clin Biomech 2020;80:105156.
[24] Lu J, Guo SC, Wang QY, Sheng JG, Tao SC. J-bone graft with double locking plate: a symphony of mechanics and biology for atrophic distal femoral non-union with bone defect. J Orthop Surg Res 2020;15:144.
[25] Eberle S, Gerber C, von Oldenburg G, Hungerer S, Augat P. Type of hip fracture determines load share in intramedullary osteosynthesis. Clin Orthop Relat Res 2009;467:1972–80.
[26] Zeng W, Liu Y, Hou X. Biomechanical evaluation of internal fixation implants for femoral neck fractures: a comparative finite element analysis. Comput Methods Progr Biomed 2020;196:105714.
[27] Zheng N, Xu J, Ruan YC, Chang L, Wang X, Yao H, et al. Magnesium facilitates the healing of atypical femoral fractures: a single-cell transcriptomic study. Mater Today 2022;52:43–62.
[28] Niinomi M. Mechanical properties of biomedical titanium alloys. Mater Sci Eng 1998;243:231–6.
[29] Wu K, Xu Y, Zhang L, Zhang Y, Xu W, Chu J, et al. Which implant is better for beginners to learn to treat geriatric intertrochanteric femur fractures: a randomised controlled trial of surgeons, metalwork, and patients. J Orthop Translat 2020;21:18–23.
[30] Simpson A, Tsang STJ. Non-union after plate fixation. Injury 2018;49(Suppl 1):S78–82.
[31] Wildemann B, Ignatius A, Leung F, Taitsman LA, Smith RM, Pesantez R, et al. Non-union bone fractures. Nat Rev Dis Prim 2021;7:57.
[32] Henderson CE, Kuhl LL, Fitzpatrick DC, Marsh JL. Locking plates for distal femur fractures: is there a problem with fracture healing? J Orthop Trauma 2011;25:S8–14.
[33] Mehboob A, Mehboob H, Ouldyerou A, Barsoum I. Computational biomechanical analysis of Ti-6Al-4V porous bone plates for lower limb fractures. Mater Des 2024;240:112842.
[34] Zhan S, Jiang D, Hu Q, Wang M, Feng C, Jia W, et al. Single-plane osteotomy model is inaccurate for evaluating the optimal strategy in treating vertical femoral neck fractures: a finite element analysis. Comput Methods Progr Biomed 2024;245:108036.
[35] Leonidou A, Moazen M, Lepetsos P, Graham SM, Macheras GA, Tsiridis E. The biomechanical effect of bone quality and fracture topography on locking plate fixation in periprosthetic femoral fractures. Injury 2015;46:213–7.
[36] Oh JK, Sahu D, Ahn YH, Lee SJ, Tsutsumi S, Hwang JH, et al. Effect of fracture gap on stability of compression plate fixation: a finite element study. J Orthop Res 2010;28:462–7.
[37] Zhang S, Patel D, Brady M, Gambill S, Theivendran K, Deshmukh S, et al. Experimental testing of fracture fixation plates: a review. Proc Inst Mech Eng H 2022;236:1253–72.
[38] Azevedo CRF. Failure analysis of a commercially pure titanium plate. Eng Fail Anal 2003;10:153–64.
[39] Stoffel K, Dieter U, Stachowiak G, Gachter A, Kuster MS. Biomechanical testing of the LCP-how can stability in locked internal fixators be controlled? Injury 2003;34(Suppl 2):B11–9.
[40] Woltz S, Duijff JW, Hoogendoorn JM, Rhemrev SJ, Breederveld RS, Schipper IB, et al. Reconstruction plates for midshaft clavicular fractures: a retrospective cohort study. Orthop Traumatol Surg Res 2016;102:25–9.
[41] Muthusamy B, Chao CK, Su SJ, Cheng CW, Lin J. Effects of merged holes, partial thread removal, and offset holes on fatigue strengths of titanium locking plates. Clin Biomech 2022;96:105663.
[42] Takizawa T, Nakayama N, Haniu H, Aoki K, Okamoto M, Nomura H, et al. Titanium fiber plates for bone tissue repair. Adv. Mater. 2018;30:1703608.

[43] Zhao D, Witte F, Lu F, Wang J, Li J, Qin L. Current status on clinical applications of magnesium-based orthopaedic implants: a review from clinical translational perspective. Biomaterials 2017;112:287–302.
[44] Wang JL, Xu JK, Hopkins C, Chow DH, Qin L. Biodegradable magnesium-based implants in orthopedics-A general review and perspectives. Adv Sci (Weinh) 2020; 7:1902443.
[45] Zhang Y, Xu J, Ruan YC, Yu MK, O'Laughlin M, Wise H, et al. Implant-derived magnesium induces local neuronal production of CGRP to improve bone-fracture healing in rats. Nat. Med. 2016;22:1160–9.
[46] Yao Z, Yuan W, Xu J, Tong W, Mi J, Ho PC, et al. Magnesium-encapsulated injectable hydrogel and 3D-engineered polycaprolactone conduit facilitate peripheral nerve regeneration. Adv Sci (Weinh) 2022;9:e2202102.
[47] Chow DHK, Wang J, Wan P, Zheng L, Ong MTY, Huang L, et al. Biodegradable magnesium pins enhanced the healing of transverse patellar fracture in rabbits. Bioact Mater 2021;6:4176–85.
[48] Zhang Q, Chen Z, Peng Y, Jin Z, Qin L. The novel magnesium-titanium hybrid cannulated screws for the treatment of vertical femoral neck fractures: biomechanical evaluation. J Orthop Translat 2023;42:127–36.
[49] Tian L, Sheng Y, Huang L, Chow DH, Chau WH, Tang N, et al. An innovative Mg/Ti hybrid fixation system developed for fracture fixation and healing enhancement at load-bearing skeletal site. Biomaterials 2018;180:173–83.